Dynamics of foam drainage

S. A. Koehler,[1] H. A. Stone,[1] M. P. Brenner,[2] and J. Eggers[3]
[1]*Division of Engineering & Applied Sciences, Harvard University, Cambridge, Massachusetts 02138*
[2]*Department of Mathematics, Massachusetts Institute of Technology, Cambridge, Massachusetts 02139*
[3]*Universität Gesamthochschule Essen, Fachbereich Physik, 45117 Essen, Germany*
(Received 10 February 1998)

The drainage of liquid foams involves the interplay of gravity, surface tension, and viscous forces. Three experimentally accessible configurations are modeled analytically using a one-dimensional nonlinear partial differential equation called the foam drainage equation: free drainage where liquid drains from an initially uniform foam of fixed length, wetting of a dry foam, and pulsed drainage where a finite blob of liquid spreads in an otherwise dry foam. Similarity solutions are described in each case and compared with numerical solutions and available experimental data. The model is generalized to higher dimensions and used to discuss further examples of pulsed drainage. [S1063-651X(98)12607-7]

PACS number(s): 47.55.Mh, 02.30.Jr, 83.70.Hq, 82.70.Rr

I. INTRODUCTION

Everyday experiences put us in direct contact with foams. Shampooing hair, washing dishes, eating chocolate bars (e.g., Three Musketeers) and chocolate mousse desserts, and pouring beer are only a few examples. There are also many industrial applications where foams are utilized in a processing stage or are part of the final product. Given the range of applications, it is not surprising that the study of foams has a long history spanning engineering, chemistry, physics, and food science (see, e.g., [1]).

It is impossible to attempt a survey of the vast literature devoted to the study of the mechanical and dynamical properties of foams. For our purposes it suffices to note that the majority of investigations have focused on aqueous foams [2], although there are now many applications of polymeric foams [3] and more recently metallic foams, which are foams made out of metals such as aluminum (see, e.g., [4]). Some commonly mentioned applications include the use of foams for reducing the impact of explosions and for cleaning up oil spills. In addition, industrial applications of polymeric foams and porous metals include their use for structural purposes (e.g., lightweight sandwich structures) and as heat exchange media analogous to common ''finned'' structures. Uniformity of the foam is important for the designer interested in these applications and since gravitational drainage of the liquid is one mechanism leading to nonuniformity, it is important to characterize the dynamics of drainage. An example of a metallic foam, with vertical nonuniformity produced by gravitational drainage, is shown in Fig. 1, which is a CAT-scan image; there are substantial variations in the liquid fraction, with the majority of the liquid residing at the bottom. In fact, we were motivated to reexamine the issue of liquid drainage in foams owing to recent interest in the manufacturing of porous metals. The reader can observe a similar drainage phenomenon in aqueous foams formed while washing dishes.

In spite of the many applications and numerous scientific investigations of the properties and mechanics of foams, the *dynamics* of foam drainage have only recently been examined in detail. In this paper we report analytical descriptions for a variety of possible drainage conditions. The major ideas and solutions presented below build upon a recently introduced one-dimensional description of an evolving foam and are described briefly next.

The subject of foam drainage was given significant impetus during the past ten years by contributions from three research groups [6–8]. In particular, a time-dependent drainage model was introduced, based upon the typical structure of aqueous foams as connected Plateau borders, which are the liquid-filled channels between three adjacent bubbles (for example, see Fig. 3). Drainage of a horizontally uniform foam was considered, so that the analytical model was for one spatial dimension. The primary dependent variable is the average (or typical) cross-sectional area A of a Plateau border, which may vary with vertical position z and time t, i.e., $A(z,t)$. The physical ingredients in the model are a conservation statement for liquid in the Plateau borders, with a fluid

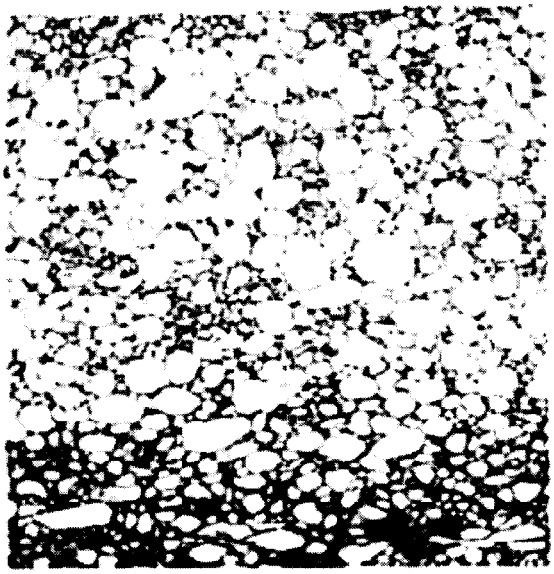

FIG. 1. CAT scan of an ALCAN aluminum foam. Dark regions indicate aluminum and light regions indicate air [5]. Drainage is evidenced by increased aluminum content at the bottom of the figure. The length of each side is 110 mm.

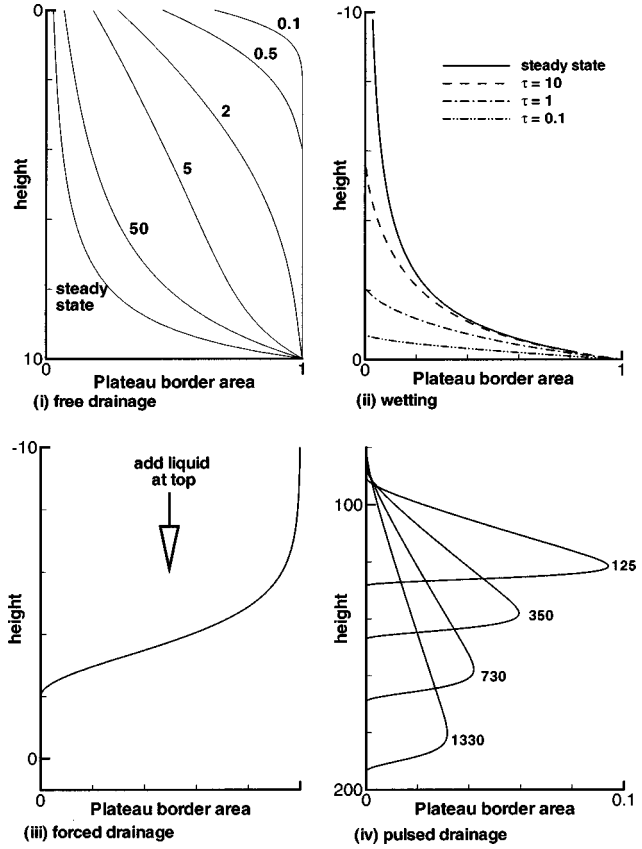

FIG. 2. Four dynamical processes in foam drainage: profiles of the Plateau border area plotted versus height. Times indicated are from the numerical solution of the dimensionless foam drainage equation as described in Sec. III. (i) Free drainage of an initially uniform foam that evolves towards the steady-state profile. (ii) Wetting of an initially dry foam from the bottom; the distribution evolves towards the steady state indicated by the solid curve. (iii) A forced drainage profile due to continual addition of liquid at the top of the foam (see, e.g., [7]); for this case the front moves at constant velocity. (iv) Pulsed drainage that shows the evolution of a finite amount of liquid in an otherwise dry foam. In cases (i) and (ii), $\alpha=1$ corresponds to the location where the foam is in direct contact with the liquid.

flux established by a competition between gravity, surface tension, and viscous forces. Physical and dimensional arguments then lead to a second-order nonlinear partial differential equation for $A(z,t)$ and several model problems have been solved either analytically or numerically. In a few cases, experiments have been performed and compared, with good results, with predictions from the one-dimensional model. We further develop these analytical ideas below. At long enough times in most foams, films that separate bubbles rupture and Ostwald ripening, due to gas diffusing through the faces between two bubbles, occurs (see, e.g., [9]). Both of these coarsening processes are neglected in the dynamical models discussed here; however, recent research has begun to address the former [10].

In many simple laboratory experiments the foam is fixed and gravitational drainage occurs relative to the fixed bubbles. Four prototypical situations may be envisioned as schematically indicated in Fig. 2: (i) free drainage of an initially uniform foam that evolves towards a steady-state profile; (ii) wetting of a foam, for example, by placing a very dry foam in contact with a liquid bath after which a spreading front forms in the foam and again evolves toward a steady-state profile; (iii) forced drainage where a constant liquid supply is added to the top of the foam and a steadily propagating front moves towards the bottom of the foam [7]; and (iv) pulsed drainage, where an initially nearly homogeneous dry foam (liquid fraction $\epsilon\approx 0$) is disturbed by the addition of a finite amount of liquid, which is then redistributed through a combination of gravitational and surface-tension-driven flows. Experimental results pertaining to cases (i), (iii), and (iv) may be found in the literature. A generalization of case (iv) is the response of a three-dimensional foam to an isolated pulse, for example, in the form of an initially cylindrical or spherical pulse.

We review the foam drainage equation in Sec. II by developing it for three-dimensional drainage problems. In Sec. III analytical descriptions are presented for one-dimensional drainage problems. We first briefly review the steady-state solution of the foam drainage equation [12]. Then, for cases (i), (ii), and (iv) we obtain similarity solutions that describe the dynamics for long times. Moreover, the analysis demonstrates that pulsed drainage (iv) combines aspects of free drainage (i), wetting (ii), and forced drainage (iii). A description of forced drainage has been described previously [11]. The spherical spreading of an isolated pulse in a dry foam is treated in Sec. IV.

II. FOAM DRAINAGE EQUATION

In several recent publications one-dimensional models for foam dynamics have been reviewed [10,12]. In the simplest version of the model, fluid is assumed to reside solely in the

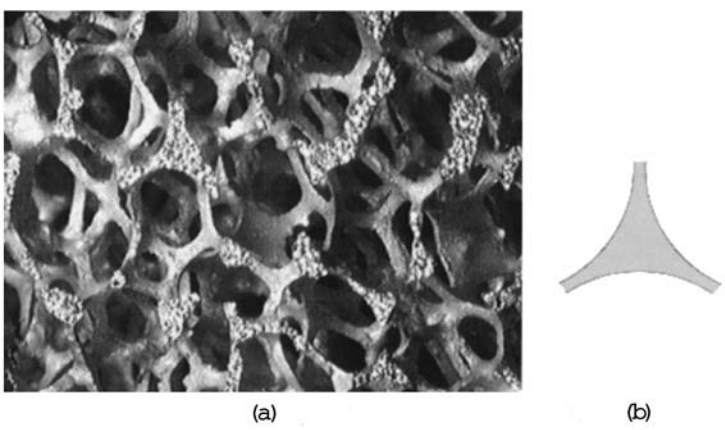

FIG. 3. (a) Network of Plateau borders of an open-cell aluminum foam [13]. The typical cell diameter is 6 mm. (b) Schematic of the cross section of a Plateau border channel through which liquid flows and whose cross-sectional area A is the basis of the foam drainage model.

Plateau borders, which are the regions where cell faces meet. Figure 3(a) shows an example of an open-cell aluminum foam composed entirely of a network of Plateau borders.

We begin by generalizing the modeling ideas to three dimensions. Because the foam is a disordered material, an average equation is derived for the typical cross-sectional area $A(\mathbf{x},t)$ of a Plateau border channel in a volume element containing many bubbles ($\mathbf{x}$ denotes the position vector); the use of such average quantities necessarily assumes an average over all possible orientations of the channels making up any small section of the foam. Of course, the usual ''continuum'' approximations are required so that the bubble size must be small relative to the typical variations of $A(\mathbf{x},t)$ in the foam for this coarse-grained description to be reasonable.

Let $\mathbf{u}$ denote the average velocity in a Plateau border channel. Then conservation of mass relates A and $\mathbf{u}$:

$$\frac{\partial A}{\partial t}+\boldsymbol{\nabla}\cdot(\mathbf{u}A)=0. \tag{1}$$

The fluid velocity $\mathbf{u}$ in these narrow channels results from a combination of three physical influences: (i) gravitationally driven drainage; (ii) capillary pressure-driven drainage due to the liquid pressure in the Plateau borders being *lower* than the pressure in the gas bubbles by an amount γ/r_c, where γ is the interfacial tension coefficient and r_c is the local radius of curvature; and (iii) viscous resistance to flow with an effective viscosity η. The average fluid velocity is determined by analogy with familiar pressure-driven viscous flows in rigid channels (e.g., Poiseuille flow). In this simplified representation, the effective viscosity accounts for the fluid's viscosity, possible interfacial rheological effects, the complicated shape of the channel cross section, and the degree to which the no-slip condition is satisfied at the fluid-gas-surfactant interface.

In particular, the local fluid motion in any given channel corresponds to a Stokes flow, which for motions of a homogeneous fluid, satisfies the equation $\mathbf{0}=-\boldsymbol{\nabla}p+\rho\mathbf{g}+\mu\nabla^2\mathbf{u}$. Further progress is then made by utilizing dimensional arguments. First, capillary effects produce a pressure gradient $-\boldsymbol{\nabla}(\gamma/r_c)$. For a foam consisting of a monodisperse collection of bubbles, on dimensional grounds, $A=\delta r_c^2$; considering the Plateau border cross section as the curved triangular area between three touching circles [shown in Fig. 3(b)], the constant is determined as $\delta=\sqrt{3}-\pi/2$. Thus the pressure gradient is $(\gamma/2)\delta^{1/2}A^{-3/2}\boldsymbol{\nabla}A$. It is important to note that the pressure gradient tends to drive fluid from regions of high A to low A, analogously to common diffusive and conductive fluxes. Second, the body force per unit volume is simply $\rho\mathbf{g}$, as for a homogeneous fluid. Third, on dimensional grounds the viscous force per unit volume acting on the fluid is approximated as $-\eta\mathbf{u}/A$, where the effective viscosity η hides much ignorance of the actual detailed flow. In effect, this phenomenological approach treats flow in the foam with a permeability equal to the Plateau border area A.

The form of the velocity then follows on dimensional grounds from Stokes equations

$$\mathbf{u}=\frac{\rho\mathbf{g}A}{\eta}-\frac{\gamma\delta^{1/2}A^{-1/2}}{2\eta}\boldsymbol{\nabla}A, \tag{2}$$

which the reader may recognize as a form of the Darcy equation for the pressure gradient described above. Thus, combining Eqs. (1) and (2), we arrive at an evolution equation for $A(\mathbf{x},t)$,

$$\frac{\partial A}{\partial t}+\frac{\rho g}{\eta}\frac{\partial A^2}{\partial z}-\frac{\gamma\delta^{1/2}}{2\eta}\boldsymbol{\nabla}\cdot(A^{1/2}\boldsymbol{\nabla}A)=0, \tag{3}$$

where z is taken as positive downward. This nonlinear second-order partial differential equation is useful for the quantitative description of foam drainage, as will be demonstrated below for one-dimensional flows and in the future for some three-dimensional foam drainage problems.

In one dimension, $A(z,t)$ only, we have

$$\frac{\partial A}{\partial t}+\frac{\rho g}{\eta}\frac{\partial A^2}{\partial z}-\frac{\gamma\delta^{1/2}}{2\eta}\frac{\partial}{\partial z}\left(A^{1/2}\frac{\partial A}{\partial z}\right)=0, \tag{4}$$

derived by Gold'farb, Kann, and Shreiber [6]. This equation has been further studied by Goldshtein, Goldfarb, and Schreiber [14] and Verbist, Weaire, and Kraynik [7,11] and has been compared to experiment in some circumstances [12,15]. Similar modeling ideas are discussed by Bhakta and Ruckenstein [8,10], who also have introduced a more detailed description of the foam at the bubble scale and incorporated surfactant effects, the role of disjoining pressure in stabilizing (or destabilizing) thin films, and bubble rupture.

As a final remark we note that with a microstructural model of the bubbles that constitute the foam the Plateau border area may be related, at least approximately, to the local volume fraction of liquid in the foam $\epsilon(\mathbf{x},t)$. If R is the ''effective'' bubble radius, then $A=c_N R^2\epsilon/(1-\epsilon)$ [8], where c_N is determined by the geometry and accounts for such features as the number of Plateau borders per bubble. In the limit of dry foams, $\epsilon\ll 1$, the foam drainage equation (3) is an evolution equation for the liquid volume fraction $\epsilon(\mathbf{x},t)$,

$$\frac{\partial\epsilon}{\partial t}+\frac{c_N R^2\rho g}{\eta}\frac{\partial\epsilon^2}{\partial z}-\frac{(c_N\delta)^{1/2}R\gamma}{2\eta}\boldsymbol{\nabla}\cdot(\epsilon^{1/2}\boldsymbol{\nabla}\epsilon)=0, \tag{5}$$

which explicitly introduces the bubble size as an additional parameter.

III. DYNAMICAL FEATURES OF DRAINAGE IN ONE DIMENSION

A. Steady state

Before discussing the dynamics of drainage, we review the steady-state profile, predicted by Eq. (4). Both the free drainage and wetting processes, described in Secs. III B and III C below, evolve towards this steady state. In the steady state, surface tension balances gravitational forcing and the fluid velocity everywhere is zero. Setting $\mathbf{u}=\mathbf{0}$ in Eq. (2) and using $A(z=L)=A_0$, one finds

$$A(z)=A_0\left[1+\frac{\rho g A_0^{1/2}}{\gamma\delta^{1/2}}(L-z)\right]^{-2}. \tag{6}$$

B. Free drainage

We begin this discussion by considering the evolution of an initially uniform foam of length L; see Fig. 2(i). Over time drainage occurs and we wish to predict $A(z,t)$. At the top of the foam $z=0$ we assume that there is zero net flux of liquid [7], which corresponds to the boundary condition

$$\rho g A^2 - \frac{\gamma \delta^{1/2} A^{1/2}}{2} \frac{\partial A}{\partial z} = 0 \quad \text{at } z=0. \tag{7}$$

Also, we are interested in those situations where the foam is characterized near the bottom $z=L$ by closely spaced spherical bubbles of radius R; for monodisperse foams the bubbles form a close-packed array in which the liquid volume fraction is expected to be approximately 26% [8] though the volume fraction can be lower for polydisperse foams. This boundary condition is closely approximated by $A(z=L,t) = \delta R^2$, which is another way that the bubble radius may enter as a parameter in a description of the drainage process. We further make the reasonable assumption that the initial state is uniform with Plateau border area $A(z,0)=A_0=\delta R^2$ [this condition must be relaxed near $z=0$ in order to satisfy the zero-flux boundary condition (7)].

Using the effective bubble radius R to scale the Plateau border area, it is then natural to define dimensionless variables according to

$$A(z,t) = \delta R^2 \alpha(\zeta,\tau), \quad z = \frac{\gamma}{2\rho g R}\,\zeta, \quad t = \frac{\eta\gamma}{2\delta R^3 (\rho g)^2}\,\tau \tag{8}$$

and so Eq. (4) may be reexpressed as the dimensionless foam drainage equation

$$\frac{\partial \alpha}{\partial \tau} + \frac{\partial \alpha^2}{\partial \zeta} - \frac{\partial}{\partial \zeta}\left(\alpha^{1/2}\frac{\partial \alpha}{\partial \zeta}\right) = 0, \tag{9}$$

where ζ and τ are, respectively, the dimensionless length and time scales. Equation (9) is to be solved subject to two boundary conditions and an initial condition

$$\alpha(\zeta>0,0)=1, \quad \alpha^{3/2}(0,\tau) - \frac{\partial}{\partial \zeta}\alpha(0,\tau) = 0,$$

$$\alpha\left(\mathcal{L} = \frac{2\rho g R L}{\gamma}, \tau\right) = 1. \tag{10}$$

Verbist, Weaire, and Kraynik [7] emphasized the importance of the free drainage limit and presented one numerical simulation of this nonlinear equation. A typical solution, generated with MATHEMATICA, is shown in Fig. 2(i) with $\mathcal{L} = 2\rho g L/\gamma = 100$ and illustrates the evolution of an initially uniform foam [16]. For long times the foam attains the steady-state profile given by the rescaled form of Eq. (6):

$$\alpha(\zeta) = \left(1 + \frac{\mathcal{L}-\zeta}{2}\right)^{-2}. \tag{11}$$

Top region of free drainage. In fact, there is a similarity solution to Eq. (9). *A priori* the similarity solution should be expected to describe the long-time ($\tau \gg 1$) features of drainage as long as externally imposed, time-independent boundary conditions are not important. In particular, Eq. (9) has the solutions

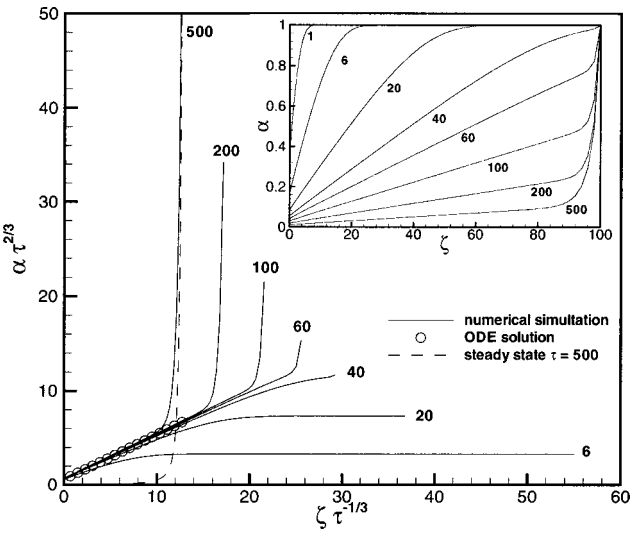

FIG. 4. Free drainage: collapse of the rescaled numerical simulation (solid curves) of Eq. (9) at times τ=6, 20, 40, 60, 100, 200, and 500; $\mathcal{L}$=100. The numerical solution of Eq. (13) for the self-similar function $\phi(s)$ is shown by the open circles. The inset shows the original numerical simulation. Note that the region of similarity space where there is good agreement corresponds to the region of physical space between the top $z=0$ and the transition region where $\alpha \to 1$. In addition, the steady-state solution (11), plotted in similarity variables at τ=500, is shown by the dashed curve. ODE denotes the solution to the ordinary differential equation (13).

$$\alpha(\zeta,\tau) = \tau^{-2/3}\phi(s) \quad \text{with } s = (\zeta - \zeta_0)\tau^{-1/3}, \tag{12}$$

where, consistently with the translational invariance of the problem, it is necessary to allow for an arbitrary offset ζ_0. This ''stagnation point'' remains at rest in similarity variables. For the no-flux boundary condition (10) to be consistent with Eq. (12), ζ_0 is at the top of the foam (i.e., $\zeta_0=0$). The similarity function $\phi(s)$ satisfies the nonlinear ordinary differential equation

$$-\tfrac{1}{3}(2\phi + s\phi') + (\phi^2)' - (\phi^{1/2}\phi')' = 0, \tag{13}$$

where $'$ indicates differentiation.

To numerically solve Eq. (13) we note that a balance of the dominant terms shows that $\phi \sim s/2$ as $s \to \infty$. It is then sufficient to choose $\phi(0)=\phi_0$, determine $\phi'(0)$ using the no-flux condition at the top of the foam (10), and integrate Eq. (13) numerically away from the origin. The choice of $\phi(0)$ is adjusted until the expected far-field asymptote $\phi \sim s/2$ is reached. Using this procedure we find $\phi(0) = 0.5885$. A comparison between the numerical solution of the original partial differential equation and the similarity solution is presented in Fig. 4 using the similarity variables to collapse the results. We note that the collapse is excellent near the top, which corresponds, as we next discuss, to $\zeta < 2\tau$. Furthermore, Weaire *et al.* (see [12], Fig. 22(b) and Eq. (10.7)) show experimentally that the slope of the free drainage profile $\partial\alpha/\partial z$ varies as 1/time, which is consistent with the above scalings (12) for $s \gg 1$.

The similarity solution (12) with numerically determined $\phi(0)$ describes the drainage profile near the top surface, but it clearly must break down as the uniform state $\alpha=1$ is approached. Since for $s\gg 1$, $\tau^{2/3}\alpha=\phi\sim\frac{1}{2}s=\frac{1}{2}\zeta\tau^{-1/3}$, the drainage profile contacts the uniform state at a distance $\zeta\approx 2\tau$ and so this approximate intersection point moves with speed 2.

Middle region of free drainage. Now we consider the manner in which the similarity solution asymptotically approaches to the uniform state $\alpha=1$ and so examine the region in the neighborhood of $\zeta\approx 2\tau$, for time short enough that the moving front has not reached the bottom, i.e., $\zeta<\mathcal{L}$. Near the moving front we expect surface tension to be important. We thus seek $\alpha(\zeta,\tau)=1+f(\zeta-2\tau,\tau)$, where $f\ll 1$, and, after substituting into Eq. (9) and neglecting terms that are smaller by $O(\tau^{-1/2})$, find

$$\frac{\partial f}{\partial\tau}+\frac{\partial f^2}{\partial\zeta_1}-\frac{\partial^2 f}{\partial\zeta_1^2}=0 \quad \text{with} \quad \zeta_1=\zeta-2\tau, \tag{14}$$

where ζ_1 is the distance from the mean location of the moving front. This equation is the Burgers equation and has a similarity solution

$$f(\zeta_1,\tau)=\tau^{-1/2}\psi(\eta_1) \quad \text{where} \quad \eta_1=\zeta_1\tau^{-1/2}, \tag{15}$$

which balances all three terms in Eq. (14) and yields

$$-\tfrac{1}{2}(\eta_1\psi)'+(\psi^2)'-\psi''=0. \tag{16}$$

Integrating once and demanding that $\psi,\psi'\to 0$ as $\eta_1\to\infty$ (i.e., the part of the profile with $\zeta\to\infty$ as $\alpha\to 1$) yields

$$\psi'=-\tfrac{1}{2}\eta_1\psi+\psi^2, \tag{17}$$

which is Bernoulli's ordinary differential equation. The solution that matches with the similarity solution described by Eq. (12) corresponds to $\psi'=\frac{1}{2}$ as $\eta_1\to-\infty$ (i.e., where $\phi\to s/2$) and is [17]

$$\psi(\eta_1)=-\frac{e^{-\eta_1^2/4}}{\int_{-\infty}^{\eta_1}e^{-\lambda^2/4}d\lambda}. \tag{18}$$

A comparison of this approximate solution and the numerical solution of the original partial differential equation (PDE) is shown in Fig. 5. The agreement is good and improves as time increases.

We have now completed the asymptotic description of free drainage for times before the moving front interacts with the lower boundary $2\tau<\mathcal{L}$. The free drainage profile has an analytical structure given by Eqs. (12) and (13) for $\zeta<2\tau$, while for the neighborhood $\zeta\approx 2\tau$ the solution is

$$\alpha(\zeta,\tau)=1-\frac{\tau^{-1/2}\exp\left[\dfrac{-(\zeta-2\tau)^2}{4\tau}\right]}{\int_{-\infty}^{(\zeta-2\tau)\tau^{-1/2}}e^{-\lambda^2/4}d\lambda}. \tag{19}$$

Finally, once the downward propagating front reaches the bottom of the foam $\zeta=\mathcal{L}$, the profile begins to evolve towards the steady-state solution (11). In Fig. 4 the steady state is indicated by the long dashed curve. We observe that the system evolves toward the steady state from the bottom up.

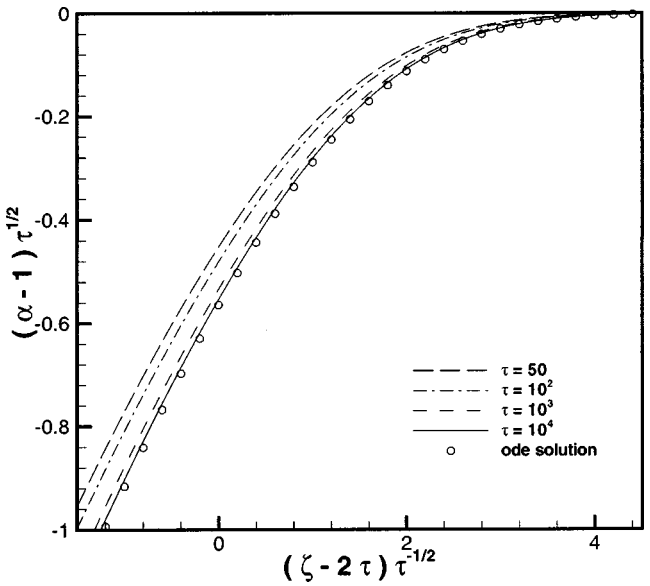

FIG. 5. Free drainage: collapse of rescaled numerical simulation (curves) for $\zeta\approx 2\tau$ and $\alpha\approx 1$. The analytical result (18) is shown by the open circles. For computational ease, the no-flux boundary condition at $z=0$ was relaxed when examining the solution near the moving front $\zeta\approx 2\tau$. Here ''ode'' solution refers to Eq. (18).

C. Wetting of a dry foam

We next describe the *wetting* of a foam, illustrated in Fig. 2(ii), as occurs, for example, when an initially dry foam is put into contact with a wetting liquid that is then ''sucked'' into the foam owing to surface-tension-driven flows. The wetting problem is analogous in some ways to the steady-state forced-drainage problem considered by Hutzler *et al.* [15] and Weaire *et al.* [12], though we shall see that its mathematical description is similar to the free-drainage problem considered in Sec. III B. The wetting process can be visualized in the laboratory by injecting liquid into the middle of a dry foam and observing the liquid rising to the top by capillarity. This one-dimensional problem may be generalized to higher dimensions by considering the evolution of a spherical initial pulse of liquid in an otherwise dry foam (Sec. IV). An experimental study of this latter problem is ongoing.

The nondimensionalization is the same as in Sec. III B and we consider solving the foam drainage equation (9) for a semi-infinite dry foam in contact with a liquid at its base. We take $\zeta=0$ to be the bottom, so that wetting occurs in the direction $\zeta<0$. The corresponding initial and boundary conditions are [18]

$$\alpha(\zeta<0,\tau=0)=0, \quad \alpha(0,\tau>0)=1, \quad \alpha(\zeta\to-\infty,\tau)\to 0. \tag{20}$$

In order to determine the long-time behavior we use the ansatz for the similarity solution of free drainage $\alpha(\zeta,\tau)=\tau^{-2/3}\phi(\zeta\tau^{-1/3})$, which then leads to Eq. (13) for $\phi(s)$. The wetting occurs out to a distance $\zeta_r(\tau)<0$, where $\alpha(\zeta_r,\tau)=0$. This moving boundary corresponds to the re-

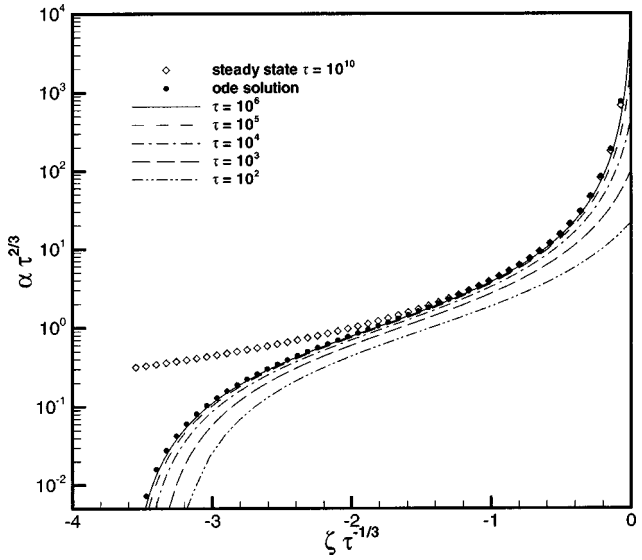

FIG. 6. Wetting of a dry foam. Numerical simulations (solid curves) of Eq. (9) and boundary condition (20) are plotted using self-similar variables for times $\tau=10^2$, 10^3, 10^4, 10^5, and 10^6. For comparison the steady-state solution (11), shown by open diamonds, was plotted at $\tau=10^{10}$. Here ''ode'' solution refers to Eq. (13).

gion that is still dry, i.e., $\alpha=0$ for $\zeta<\zeta_r(\tau)$. We thus look for solutions with $\phi(s_r)=0$, where $s_r=\zeta_r\tau^{-1/3}$. A local analysis of Eq. (13) near such an s_r reveals that ϕ must have the power series form

$$\phi=b_1(s-s_r)^2+b_2(s-s_r)^3+\cdots. \tag{21}$$

The coefficients b_1 and b_2 are found to be

$$b_1^{1/2}=-\frac{s_r}{6}, \quad b_2=\frac{s_r}{27}. \tag{22}$$

In particular, this result means that s_r must be negative, as expected, so that in physical space the point of touchdown is

$$\zeta_r=s_r\tau^{1/3}. \tag{23}$$

For long times $\tau\gg1$, we observe that $\phi(s)$ satisfies the two boundary conditions $\phi(0)\to\infty$ and $\phi(s_r)=0$; s_r is found numerically to be $s_r=-3.620$.

Figure 6 displays the numerical simulation of the partial differential equation for wetting of a dry foam. The axes were rescaled to the self-similar ansatz (12) to show the collapse of the numerical data at long times. The profile evolves towards the steady-state solution (symbols), which has been plotted for the time $\tau=10^{10}$ and we observe that deviations from the steady state occur for $\zeta<-2\tau^{1/3}$. The steady state is in fact contained as a special case since the similarity solution converges to it at fixed ζ as $\tau\to\infty$.

D. Pulsed drainage

Verbist, Weaire, and Kraynik [7] perform a second form of drainage experiment: pulsed drainage in an otherwise nearly dry foam. During a short-time interval, a fixed amount of liquid is injected into a vertical foam. The (horizontally uniform) pulse then travels down the foam and spreads vertically; see Fig. 2(iv). In this section we predict analytically the spreading rate and profile of the pulse using similarity solutions that are expected to capture the long-time behavior starting with arbitrary initial conditions. The detailed structure of the spreading pulse has a main body that translates primarily owing to the gravitational body force, while at the front and rear of the pulse surface tension effects are significant.

We begin with the dimensional form of the foam drainage equation (4). If we assume that the background foam is nearly dry, then Eq. (4) is to be solved subject to the global mass balance

$$\int_{z_r(t)}^{z_f(t)}A(z,t)dz=V_{\rm liq}, \tag{24}$$

where $V_{\rm liq}=V_{\rm tot}/nRS$. Here $V_{\rm tot}$ is the injected liquid volume of the pulse, n is the number of Plateau borders per unit volume of the foam, R is a typical bubble radius (i.e., the height of a Plateau border), and S is the cross-sectional area of the one-dimensional flow experiment. Also, $z_r(t)$ and $z_f(t)$ denote, respectively, the back and front locations of the spreading pulse. In fact, Eq. (4) has the same mathematical structure as the equation that describes the shape of a drop spreading on an inclined plane, except that the detailed form of the surface tension term is modified. The gravitational and surface-tension-driven evolution of such a drop was described by Huppert [19] and Troian *et al.* [20], who demonstrated that the large-scale features of the drop spreading could be characterized by similarity solutions (see also [21] and [22]). Not surprisingly, we also find similarity solutions for the foam drainage problem, though there are additional structural differences in the solutions as contrasted with those in the previous studies of drop spreading.

It is convenient to first nondimensionalize by scaling area, vertical height, and time according to

$$A(z,t)=\frac{4V_{\rm liq}^2}{\delta}\left(\frac{\rho g}{\gamma}\right)^2\alpha(\zeta,\tau), \quad z=\frac{\delta}{4V_{\rm liq}}\left(\frac{\gamma}{\rho g}\right)^2\zeta,$$

$$t=\frac{\eta\delta^2}{16\rho g V_{\rm liq}^3}\left(\frac{\gamma}{\rho g}\right)^4\tau, \tag{25}$$

so that the dimensionless form of the problem is

$$\frac{\partial\alpha}{\partial\tau}+\frac{\partial\alpha^2}{\partial\zeta}-\frac{\partial}{\partial\zeta}\left(\alpha^{1/2}\frac{\partial\alpha}{\partial\zeta}\right)=0, \quad \int_{\zeta_r(\tau)}^{\zeta_f(r)}\alpha(\zeta,\tau)d\zeta=1. \tag{26}$$

A typical numerical solution of Eq. (26) is shown in Fig. 2(iv). The initial condition was a localized Gaussian shape with unit volume. The asymmetric spreading of the pulse is apparent.

Main body of the pulse. We now seek to describe analytically the time-dependent evolution of the pulse and are primarily interested in the behavior at long times $\tau\gg1$ when the details of the initial distribution are lost. In particular, following the spirit of Huppert's analysis and motivated by the numerical solutions shown in Fig. 2(iv), we observe that throughout most of the pulse the gravitational body force is more important than the surface tension driving force:

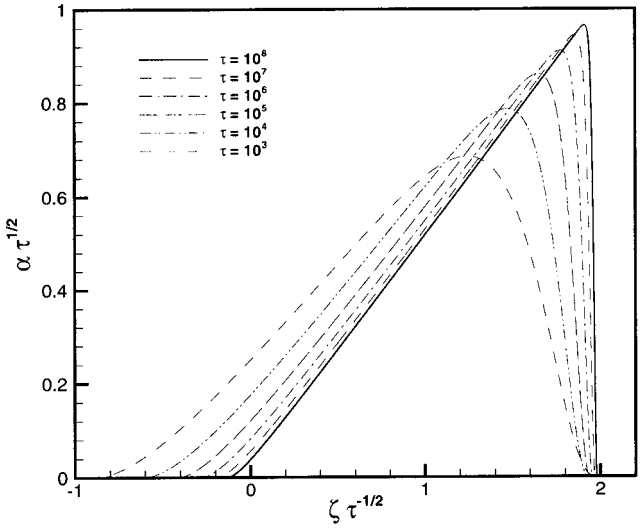

FIG. 7. Pulsed drainage profiles rescaled using similarity variables appropriate to the middle of the pulse, where surface tension is not significant.

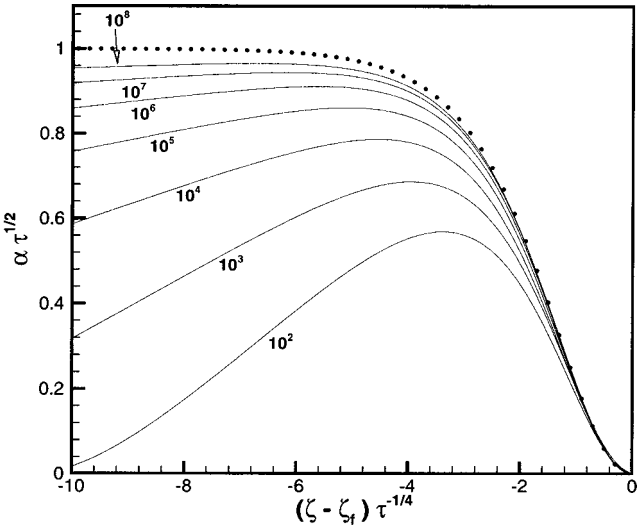

FIG. 8. Rescaling of the pulsed drainage PDE simulations (curves) focusing on the profile near the front; collapse of the numerical results onto the analytical result (34), here denoted by the dots.

$$\frac{\partial \alpha}{\partial \tau}+\frac{\partial \alpha^2}{\partial \zeta}=0. \tag{27}$$

This equation may be solved using the method of characteristics and for long times the solution has the form

$$\alpha(\zeta,\tau)=\frac{(\zeta-\zeta_0)}{2\tau}, \tag{28}$$

where ζ_0 sets the location of the rear of the pulse. Using global mass conservation and assuming that $|\zeta_f| \gg |\zeta_r|$ shows that the foam pulse has a finite length that increases as $O(\tau^{1/2})$ and the Plateau border area in the immediate neighborhood of the front (α_f) decreases as $O(\tau^{-1/2})$; in detail

$$\zeta_f(\tau)=2\tau^{1/2}, \quad \alpha_f(\tau)=\alpha(\zeta_f(\tau),\tau)=\tau^{-1/2}. \tag{29}$$

Throughout this central/forward region of nonzero α the surface tension term in Eq. (4) is smaller by $O(\tau^{-1/4})$ for $\tau \gg 1$. A comparison between this similarity solution and the full numerical solution is shown in Fig. 7 and collapse of the data for long times is observed. The two power laws (29) have been observed in recent experimental measurements (see [12], Figs. 23b and 23c; see also Eqs. 8.6 and 8.7 therein). Furthermore, applying the same treatment as used to collapse the numerical simulations shown in Fig. 7 according to Eq. (29), we found good qualitative collapse of the Weaire *et al.* [12] pulsed drainage measurements shown in their Fig. 23(a).

Front of the pulse. The above results describe the major features of the middle of the spreading pulse. Surface tension acts to smooth and further spread both the front and the rear of the pulse. In order to examine the front in more detail we return to Eq. (26) and transform to a coordinate system moving with the location of the front $\zeta \approx \zeta_f(\tau)$ and $\alpha \approx \alpha_f(\tau)$ [see Eq. (29)]:

$$\alpha(\zeta,\tau)=\alpha_f(\tau)a(\xi) \quad \text{where} \quad \xi=\frac{\zeta_f(\tau)-\zeta}{c(\tau)}. \tag{30}$$

We thus seek the similarity function $a(\xi)$. For long times we obtain a self-consistent asymptotic balance if we identify

$$c(\tau)=\tau^{1/4}, \tag{31}$$

after which the foam drainage equation simplifies to the ordinary differential equation

$$a'-(a^2)'-(a^{1/2}a')'=0, \tag{32}$$

where the neglected terms are smaller by $O(\tau^{-1/4})$ as $\tau \to \infty$. Equation (32) can be integrated once and, since $a \to 1$ and $a' \to 0$ as $\xi \to \infty$, then the integration constant is set to zero. Thus

$$a'=(1-a)a^{1/2}, \tag{33}$$

which may be integrated with $a(0)=0$ to arrive at

$$a(\xi)=\tanh^2(\xi/2),$$

which implies

$$\alpha(\zeta,\tau)=\tau^{-1/2}\tanh^2\left(\frac{2\tau^{1/2}-\zeta}{\tau^{1/4}}\right), \tag{34}$$

or in dimensional form

$$A(z,t)=\left(\frac{\eta V_{\mathrm{liq}}}{\rho g}\right)^{1/2} t^{-1/2}\tanh^2\left(\frac{2[(\rho g)^2\eta V_{\mathrm{liq}}]^{1/4}[z_f(t)-z]}{\gamma\delta^{1/4}t^{1/4}}\right). \tag{35}$$

The width of the front thus increases in time proportionally to $\tau^{1/4}$. We also note that this $\tanh^2$ solution has the same form as the forced drainage result discussed by Hutzler *et al.* [15], which also compared favorably with their forced-drainage experiments. The physics underlying this similarity between pulsed and forced drainage is that the nose of a traveling pulse is locally determined and thus has essentially the same shape as the forced drainage front profile. In Fig. 8

we rescale the results from the numerical simulations to show that the front of the pulse evolves towards the prediction of Eq. (34).

Rear of the pulse. After finding these solutions that describe the evolution of the middle and front of the pulse, we now turn to the rear of the pulse. In this region, both surface tension and gravity are important and, in fact, this problem is very similar to the wetting process described in Sec. III C. We therefore look for a similarity solution of the form given in Eq. (12), which was encountered in the discussion of free drainage and so now seek $\phi(s)$. One of the boundary conditions for this problem will be supplied by matching the gravity-driven solution (28) valid as one moves toward the front of the pulse.

Following the analysis outlined in the description of wetting, we look for solutions with $\phi(s_r)=0$ at some finite s_r. A local analysis of Eq. (13) has the same form as for wetting, i.e., $\phi=b_1(s-s_r)^2+b_2(s-s_r)^3+\cdots$. Now, however, the rear touchdown point $\zeta_r(\tau)$ corresponds to $\zeta_r=\zeta_0+s_r\tau^{1/3}$, where s_r is determined numerically and, owing to different boundary conditions, has a different value from before.

Equations (21) and (22) provide us with a family of solutions, parametrized only by s_r. This remaining parameter is fixed by matching onto the known solution (28), which in similarity space has the form

$$\phi(s)\approx s/2 \quad \text{as} \quad s\to\infty. \tag{36}$$

Direct substitution of Eq. (36) into the similarity differential equation confirms that surface tension is asymptotically negligible away from the rear, which is the region where the gravitational body force dominates [middle section; see Fig. 2(iv)], as discussed earlier in this section. Now s_r can be adjusted such that the corresponding solution of Eq. (13), numerically integrated towards positive ζ (or ξ), conforms with Eq. (36). Since the asymptotic behavior of Eq. (13) is unstable, the numerical solutions with an incorrect s_r veer off to plus or minus infinity. Via an iterative procedure, we numerically find $s_r\approx -2.898$.

We verified the validity of this solution by comparing with a numerical solution of Eq. (9). As initial conditions we chose a narrow Gaussian pulse, which is allowed to evolve [18]. To obtain a proper fit, the point ζ_0 in Eq. (12) still needs to be determined and should not be confused with the initial position of the pulse. From Eq. (12) the equation for ζ_0 is

$$\alpha(\zeta_0,\tau)=\tau^{2/3}\phi(0). \tag{37}$$

This condition uniquely defines a point ζ_0 in space, which for large τ turns out to be stationary as it must for self-consistency of the similarity approach. In contrast to free drainage $\phi(s=0)=0.820$ and the flux through the point ζ_0 decays as $O(\tau^{-4/3})$. With these ideas we can plot the simulation results in similarity variables $s=(\zeta-\zeta_0)/\tau^{1/3}$, as shown in Fig. 9, which illustrates that rescaling about this fixed point collapses the rear and middle of the pulse.

Finally, in Fig. 10 we summarize results for the time dependence of the moving boundaries in the pulse evolution. Included in the plot are the motion ζ_f of the pulse front with time, the location ζ_r of the rear of the profile that wets the dry foam in the direction of negative z, and the location $\zeta_{\max}$ of the maximum of α. All the scaling estimates, deduced from long-time similarity solutions, are in excellent agreement with the numerical results.

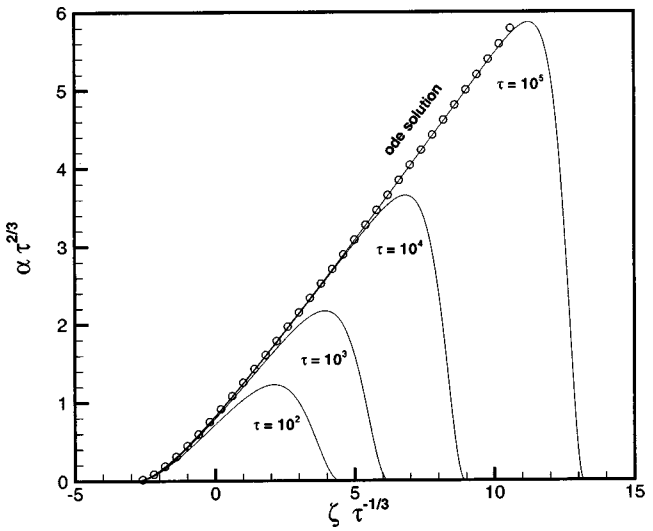

FIG. 9. Pulsed drainage near the rear: collapse of rescaled numerical simulations (curves) onto the exact ODE solution (12) (open circles) at times $\tau=10^2$, 10^3, 10^4, and 10^5.

IV. GENERALIZATION OF THE PULSED SOLUTIONS TO HIGHER DIMENSIONS: THE GRAVITY-FREE CASE

In the absence of significant gravitational influences, which is expected to be closely approximated in the microgravity environment characteristic of handling materials in space, the motion of the liquid in the foam is governed by

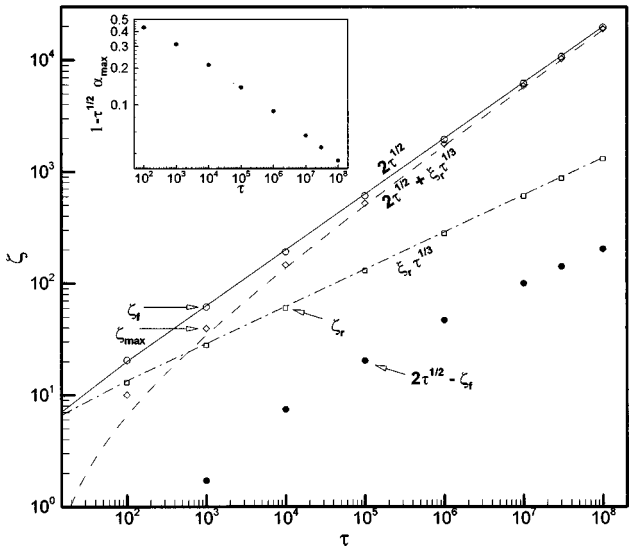

FIG. 10. ''Moving boundaries'' in pulsed drainage. Numerical results are shown by symbols and asymptotic approximations are shown as curves. The time dependences correspond to motion of the pulse front $\zeta_f\approx 2\tau^{1/2}$, the rear $\zeta_r\approx\xi_r\tau^{1/3}$, and the position of the maximum of the pulse $\zeta_{\max}=2\tau^{1/2}+\xi_r\tau^{1/3}+O(\tau^{1/4})$. The solid circles show an $O(\tau^{1/4})$ deviation from the simple estimate $\zeta_f\approx 2\tau^{1/2}$. The inset shows that the pulse height obeys $\alpha_f(\tau)=\tau^{-1/2}[1+O(\tau^{-1/4})]$.

surface tension. The evolution of such an isolated pulse in one dimension was described by Gold'farb, Kann, and Shreiber [6]. The generalization to two and three dimensions is straightforward and corresponds, respectively, to otherwise dry foams with a localized wet domain in the shape of a cylindrical or spherical blob.

For this aspect of our work it is convenient to utilize the liquid volume fraction $\epsilon(\mathbf{x},t)$ as described in Sec. II. Then, in the absence of gravitational effects of $\mathbf{g}$ and seeking symmetric solutions $\epsilon(r,t)$, we write Eq. (5) as

$$\frac{\partial \epsilon}{\partial t}=\frac{(c_N\delta)^{1/2}R\gamma}{2\eta r^{d-1}}\frac{\partial}{\partial r}\left(\epsilon^{1/2}r^{d-1}\frac{\partial \epsilon}{\partial r}\right), \tag{38}$$

where $d=1,2,3$ in one, two, and three dimensions, respectively. This is a nonlinear diffusion equation with ''diffusivity'' $D=(c_N\delta)^{1/2}R\gamma/2\eta$. The evolution of an isolated pulse on an otherwise dry foam must also conserve volume, which requires in d dimensions

$$\int_0^{l(t)}\epsilon(r,t)r^{d-1}dr=q/c_d, \tag{39}$$

where $c_d=2,2\pi,4\pi$ for $d=1,2,3$, respectively, and q is the appropriate dimensional ''volume'' consistent with the problem statement. There is a standard solution approach for this class of nonlinear diffusion problems.

The pulse evolves in time and solutions to this nonlinear partial differential equation are found with $\phi\equiv 0$ for $r>l(t)$. This problem has similarity solutions of the form

$$\epsilon(r,t)=\left[\frac{4q^{4/d}}{(d+4)^2D^2c_d^{4/d}}\right]^{d/(d+4)}t^{-2d/(d+4)}\phi(s), \tag{40a}$$

where

$$s=\frac{r}{c_1t^{2/(d+4)}},\quad c_1=\left[\frac{(d+4)^2qD^2}{4c_d}\right]^{1/(d+4)}. \tag{40b}$$

Substitution into Eq. (38) shows that $\phi(s)$ satisfies

$$-(s^d\phi)'=(\phi^{1/2}s^{d-1}\phi')'. \tag{41}$$

Integrating twice and using the boundary conditions that $\phi(0)$ is bounded and $\phi(s_l)=0$, where $l(t)=s_lt^{2/(d+4)}$ defines the finite wetted region, yields the solution

$$\phi(s)=\tfrac{1}{16}(s_l^2-s^2)^2. \tag{42}$$

Substitution into the volume conservation statement (39) yields

$$s_l=\left[\frac{1}{16}\int_0^1(1-s^2)s^d ds\right]^{-1/(d+4)}$$
$$=[2d(d+2)(d+4)]^{1/(d+4)}. \tag{43}$$

Therefore, we see that the pulse spreads at a rate $t^{2/(d+4)}$ and decreases at a rate $t^{-2d/(d+4)}$. We are currently trying to study similar problems experimentally.

V. CONCLUDING REMARKS

We have presented similarity solutions to the foam drainage equation for several experimentally accessible configurations. The analytical results are in excellent agreement with numerical simulations of the governing partial differential equation, and quantitatively agree with experimental data. The case of wetting a dry foam and extensions of the foam drainage equation to higher dimensions were discussed also.

In particular, we treated free drainage, wetting, and pulsed drainage processes. One common feature is that the pulsed drainage profile consists of three distinct regions: an advancing nose, which is similar to forced drainage, that spreads in time as $O(\tau^{1/4})$ and an advancing rear, which is similar to wetting, that spreads in time as $O(\tau^{1/3})$; these two regions share a middle region, containing the maximum of the pulse, which decreases with time as $O(\tau^{-1/2})$ and spreads as $O(\tau^{1/2})$.

ACKNOWLEDGMENTS

We thank A. Evans for guidance and suggestions, A. Evans, H. Wadley, J. Woods, and H. Sang for helpful conversations, D. Sypeck for the CAT-scan image in Fig. 1, A. Bastawros for the ERG photograph in Fig. 2, and J. Lister for bringing Ref. [21] to our attention. Support from ONR Grant No. N00014-1-96-1028 is gratefully acknowledged. Also, we thank D. Weaire and S. Hutzler for providing us with preprints of their research.

[1] K. J. Mysels, K. Shinoda, and S. Frankel, *Soap Films: Studies of their Thinning* (Pergamon, Oxford, 1959).
[2] R. Prud'homme and S. Khan, *Foams: Theory, Measurements and Applications* (Dekker, New York, 1996).
[3] L. J. Gibson and M. F. Ashby, *Cellular Solids: Structure & Properties* (Cambridge University Press, Cambridge, 1997).
[4] J. Banhart, *Metallschäume* (MIT-Verlag, Bremen, 1997).
[5] D. J. Sypeck, H. N. G. Wadley, H. Bart-Smith, S. A. Koehler, and A. G. Evans, *Review of Progress in Quantitative Nondestructive Evaluation*, edited by D. O. Thompson and D. E. Chimenti (Plenum, New York, 1998), Vol. 17.
[6] I. I. Gol'dfarb, K. B. Kann, and I. R. Shreiber, Izv. Akad. Nauk SSSR **2**, 103 (1988).
[7] G. Verbist, D. Weaire, and A. M. Kraynik, J. Phys.: Condens. Matter **8**, 3715 (1996).
[8] A. Bhakta and E. Ruckenstein, Langmuir **11**, 1486 (1995).
[9] D. J. Durian, D. A. Weitz, and D. J. Pine, Science **252**, 686 (1991).
[10] A. Bhakta and E. Ruckenstein, Adv. Colloid Interface Sci. **70**, 1 (1997).
[11] G. Verbist and D. Weaire, Europhys. Lett. **26**, 631 (1994).
[12] D. Weaire, S. Hutzler, G. Verbist, and E. Peters, Adv. Chem. Phys. **102**, 315 (1997).
[13] Energy Research and Generation, Inc., Oakland, CA 94608.
[14] V. Goldshtein, I. Goldfarb, and I. Schreiber, Int. J. Multiphase Flow **22**, 991 (1996).

[15] S. Hutzler, G. Verbist, D. Weaire, and J. A. van der Steen, Europhys. Lett. **31**, 497 (1995).

[16] Note that in order to begin the simulation, the initial profile was selected to obey the no-flux boundary condition (7) at $z=0$ and quickly transition to $\alpha=1$. We chose

$$\alpha(\zeta,\tau=0)=\left\{1+b\left[\tanh\left(\frac{\zeta(1-b)^2}{2b}\right)-1\right]\right\}^2,$$

where b determines the width of the transition. Typically we chose $b=0.1$.

[17] I. Mezić pointed out to us the connection with the Burgers equation. In fact, an almost identical mathematical problem can be found in P. G. Drazin and R. S. Johnson, *Solitons: An Introduction* (Cambridge University Press, Cambridge, 1989), p. 34, Q2.8.

[18] For computational purposes, ''dry'' corresponds to a small constant background value of $\alpha=10^{-8}$. This is physically reasonable since foams always have some nonzero liquid content.

[19] H. Huppert, Nature (London) **300**, 427 (1982).

[20] S. M. Troian, E. Herbolzheimer, S. A. Safran, and J. F. Joanny, Europhys. Lett. **10**, 25 (1989).

[21] R. E. Grundy, IMA J. Appl. Math. **31**, 121 (1983).

[22] A. L. Bertozzi and M. P. Brenner, Phys. Fluids **9**, 530 (1997).